Metamagnetism of Weakly Coupled Antiferromagnetic Topological Insulators

Aoyu Tan,[1,2] Valentin Labracherie,[1,2] Narayan Kunchur,[2] Anja U. B. Wolter,[2] Joaquin Cornejo,[2] Joseph Dufouleur,[2,3] Bernd Büchner,[2,4] Anna Isaeva,[2,4] and Romain Giraud[1,2]

[1]*Université Grenoble Alpes, CNRS, CEA, Spintec, F-38000 Grenoble, France*
[2]*Institute for Solid State Physics, Leibniz IFW Dresden, D-01069 Dresden, Germany*
[3]*Center for Transport and Devices, Technische Universität Dresden, D-01069 Dresden, Germany*
[4]*Institut für Festkörperphysik and Würzburg-Dresden Cluster of Excellence ct.qmat, Technische Universität Dresden, 01062 Dresden, Germany*

(Received 8 January 2020; revised manuscript received 27 February 2020; accepted 14 April 2020; published 13 May 2020)

The magnetic properties of the van der Waals magnetic topological insulators $MnBi_2Te_4$ and $MnBi_4Te_7$ are investigated by magnetotransport measurements. We evidence that the relative strength of the interlayer exchange coupling J to the uniaxial anisotropy K controls a transition from an A-type antiferromagnetic order to a ferromagneticlike metamagnetic state. A bilayer Stoner-Wohlfarth model allows us to describe this evolution, as well as the typical angular dependence of specific signatures, such as the spin-flop transition of the uniaxial antiferromagnet and the switching field of the metamagnet.

DOI: 10.1103/PhysRevLett.124.197201

The coexistence of large spin-orbit and exchange couplings in 3D crystals can lead to a variety of topological electronic phases, some of which being tunable by changing the magnetic order parameter (orientation, amplitude) or the micromagnetic structure [1–4]. This requires the accurate control of the magnetic properties, however, also at the microscopic level. A breakthrough was the discovery of the quantum anomalous Hall (QAH) state in diluted magnetic topological insulators [5], with dissipationless edge states induced by the magnetization. Because of a small energy gap of the surface-state band structure, the Hall resistance quantization is only observed at subkelvin temperatures [6–9].

Recently, stoichiometric magnets have raised specific interest [10–13], with the possibility of tailoring multilayers of exchange-coupled 2D ferromagnets having a nontrivial band structure and larger gaps. In particular, $MnBi_2Te_4$ was evidenced as the first antiferromagnetic topological insulator, with a Néel temperature $T_N = 24$ K [12,14–18]. In addition, novel topological phases and transitions were predicted in antiferromagnets [2,19], as well as parity effects in thin magnetic multilayers [20,21]. Theoretical predictions also considered other topological phases in the bulk, such as magnetic Weyl semimetals or axion electrodynamics [20,22,23]. In all cases, the control of a topological state is directly related to that of the micromagnetic structure, and the quantized Hall state was observed in large magnetic fields only [24–26]. Importantly, van der Waals multilayers of 2D ferromagnets offer the possibility to modify the interlayer exchange coupling J, with nonmagnetic spacers, whereas the single-layer magnetic anisotropy K remains barely affected. This can be achieved in the so-called MBT family, $[MnBi_2Te_4][Bi_2Te_3]_n$ with the integer $n \geq 0$, that ideally realizes stoichiometric magnetic topological insulators [14,21,27–33]. The magnetic base unit, a single $MnBi_2Te_4$ septuple layer, is a 2D ferromagnet (intralayer coupling $J_F < 0$) with a perpendicular anisotropy K_U that stabilizes an out-of-plane ferromagnetic order and generates the QAH state. Stacks of septuple layers form the $MnBi_2Te_4$ compound, with an antiferromagnetic interlayer coupling ($J = J_{AF} > 0$). It is also possible to grow related crystals that have n units of the nonmagnetic Bi_2Te_3 spacer in between 2D ferromagnetic layers and therefore a reduced exchange coupling J.

In this Letter, we evidence that such crystalline MBT magnetic multilayers are actually textbook systems that realize the weak-coupling regime of uniaxial antiferromagnets, except $MnBi_2Te_4$, with robust metamagnetic properties controlled by their perpendicular anisotropy. To evidence this behavior, we investigated the magnetic properties of Hall-bar-shaped nanostructures of both $MnBi_2Te_4$ and $MnBi_4Te_7$, in a comparative study, by magnetotransport measurements. Below their Néel temperature, the typical signature of an A-type collinear antiferromagnet, a spin-flop transition, is observed. However, $MnBi_4Te_7$ undergoes another transition to a bistable metamagnetic state at lower temperatures, with a fully saturated remnant magnetization below about 3 K and abrupt spin-flip transitions. This evolution is well described by a magnetic bilayer Stoner-Wohlfarth model with an interlayer exchange coupling J and a temperature-dependent effective anisotropy K related to the single-layer uniaxial anisotropy K_U. Our model also reproduces the angular dependence of these different magnetic states under a tilted

magnetic field. This finding of metamagnetism is very general for van der Waals 2D-layered ferromagnets with a weak interlayer exchange coupling as compared to their uniaxial anisotropy strength. In the limit of a large K/J ratio, the model suggests a direct phase transition from paramagnetism to metamagnetism, with a saturated magnetization at remanence up to the blocking temperature T_B of the 2D ferromagnet base unit, with an upper bond given by the critical temperature of the magnetic base unit. This situation is realized for both $MnBi_4Te_7$ ($n = 1$) and $MnBi_6Te_{10}$ ($n = 2$), for which magnetic hysteresis was observed but interpreted in terms of a ferromagnetic state [29–31]. Our study actually shows the importance of both the *intralayer* 2D exchange coupling J_F and the *perpendicular anisotropy* K_U to realize robust metamagnetic states and to stabilize the QAH regime at higher temperatures. Furthermore, our model is very general and can be applied to other weakly coupled magnetic multilayers with a perpendicular anisotropy, such as novel van der Waals magnetic heterostructures [34].

Nanoflakes of both $MnBi_2Te_4$ and $MnBi_4Te_7$ were obtained by mechanical exfoliation of large single crystals, the bulk properties of which are reported elsewhere [14,28,35,36]. Nanostructures were transferred onto a SiO_2/Si^{++} substrate, and then further processed by e-beam lithography to prepare Cr/Au Ohmic contacts and then shaped into a Hall-bar geometry. Magnetotransport measurements were performed with ac lock-in amplifiers, using a small polarization current, down to very low temperatures ($T > 70$ mK) and in an Oxford Instruments 3D-vector 2T magnet. High-field measurements, up to 14 T, were realized in a variable-temperature insert, down to 1.8 K, at different magnetic field orientations by using a mechanical rotator.

Both $MnBi_2Te_4$ and $MnBi_4Te_7$ nanoflakes showed a dirty metal-like behavior due to disorder (see Supplemental Material [37]). Moreover, the average carrier mobility is reduced by spin-dependent scattering at a phase transition to a Néel antiferromagnetic state, giving a resistivity peak at the critical temperature T_N (maximum of magnetic fluctuations), with $T_N = 23.5(5)$ and $T_N = 12.5(5)$ K, respectively. A simple mean-field model analysis already reveals the much reduced interlayer exchange coupling J_{AF} in $MnBi_4Te_7$ compared to $MnBi_2Te_4$. The magnetic susceptibility above T_N gives a paramagnetic Weiss temperature $\theta_P = 1(1)$ K for $MnBi_2Te_4$ and $\theta_P = 12(1)$ K for $MnBi_4Te_7$ [14,28,29,31,36]. Since the ratio θ_P/T_N is given by $[(J_F + J_{AF})/(J_F - J_{AF})]$ [38], this shows that $J_{AF}/J_F \approx -0.92$ for $MnBi_2Te_4$ and $J_{AF}/J_F \approx -0.04$ for $MnBi_4Te_7$. All MBT-n compounds are therefore weakly coupled 2D magnetic multilayers ($J_{AF} \ll |J_F|$), apart from $MnBi_2Te_4$, which has $J_{AF} \lesssim |J_F|$. Below T_N, the resistivity is reduced upon cooling the sample, as magnons are progressively frozen. More evidence of the weaker interlayer coupling in $MnBi_4Te_7$ is thus given by the faster decrease of the resistivity with decreasing the temperature, since 2D magnetic fluctuations are efficiently gapped by the uniaxial anisotropy.

A clear signature of the collinear A-type antiferromagnetic state is further observed in the magnetoresistance. In zero magnetic field, the two sublattice magnetizations are aligned along the uniaxial anisotropy axis perpendicular to the septuple plane. If the field is applied along the easy axis, the magnetoresistance shows a reversible curve with a peak at the spin-flop transition, specific to a uniaxial antiferromagnet with a dominant exchange energy, when sublattice magnetizations suddenly evolve to a canted state due to the finite antiferromagnetic coupling and anisotropy [38]. The temperature dependence of the spin-flop field $H_{SF} \propto \sqrt{JK}$ is related to that of the effective anisotropy $K = K_U/M_S^2 * \langle M_Z^2 \rangle$, where M_Z and M_S are the perpendicular and saturated magnetization, respectively, and $\langle\rangle$ is the thermal average. As magnetic fluctuations are reduced at lower temperatures, the effective uniaxial anisotropy K increases and so does the spin-flop field below T_N. However, there are some striking differences between both magnets at lower temperatures, due to the relative strength of the exchange field $H_{exch} \propto J$ compared to the anisotropy field $H_A \propto K$. For $MnBi_2Te_4$, J is always larger than K. This leads to the features seen in Fig. 1(a). First, the spin-flop field is smaller than the saturation field, the latter being solely determined by the exchange field if the field is applied along the anisotropy axis. Second, the spin-flop transition induces a large canting of the magnetization with respect to the uniaxial anisotropy direction, which results in a visible contribution from the negative anisotropic magnetoresistance. This evolution of the magnetization is indeed confirmed by that of the anomalous Hall resistance, which is a measure of the magnetization component M_Z perpendicular to the sample plane (see Supplemental Material [37]). At higher fields, the magnetization slowly realigns toward the anisotropy axis and the resistance increases again, up to the magnetization saturation field that is clearly observed as a kink in the magnetoresistance. At even larger fields, only the cyclotron magnetoresistance remains. The angular dependence with a tilted magnetic field confirms this scenario,

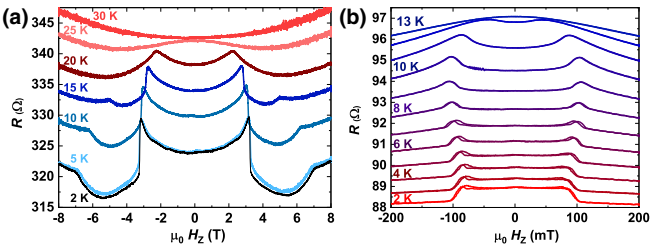

FIG. 1. Temperature dependence of the magnetoresistance for (a) $MnBi_2Te_4$ and (b) $MnBi_4Te_7$, with peaks at the magnetization reversal (spin-flop or spin-flip transitions) below (a) $T_N = 23.5(5)$ and (b) $T_N = 12.5(5)$ K. The perpendicular field H_Z is parallel to the easy-anisotropy axis. Curves are shifted for clarity.

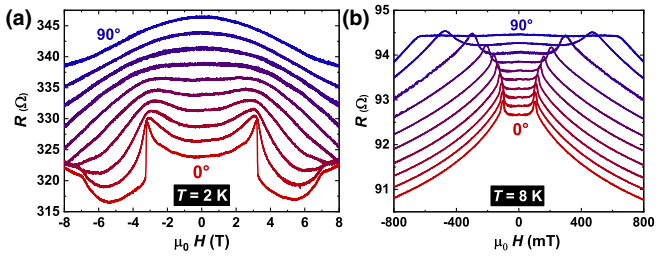

FIG. 2. Angular dependence of the magnetoresistance for (a) $MnBi_2Te_4$, showing the fast vanishing of the spin-flop transition for all temperatures down to $T = 2$ K, and for (b) $MnBi_4Te_7$, showing the smooth evolution of the spin-flop transition measured at $T = 8$ K. Curves with a 10° step are shifted for clarity.

with the rapid vanishing of the spin-flop event and the sole contribution of the anisotropic magnetoresistance at large angles [Fig. 2(a)]. For $MnBi_4Te_7$, we found two different regimes. Below T_N and above about $T = 8$ K, the magnetic properties are also those of a uniaxial antiferromagnet, with a resistance peak at the spin-flop transition [Fig. 1(b)]. The spin-flop transition is, however, observed at a much smaller field, as expected due to the reduced interlayer coupling J. Considering the anisotropy is determined locally within a septuple layer, and is therefore similar for both compounds, this would give a ratio $H_{SF}^{124}/H_{SF}^{147} \approx 5$, whereas it is about 30 since $B_{SF}^{124} \approx 3$ T and $B_{SF}^{147} \approx 100$ mT. This difference is already a sign that the nature of the magnetization reversal changes in $MnBi_4Te_7$, as the anisotropy energy becomes larger than the exchange energy. As a consequence, H_{SF}^{147} has a smooth angular dependence [Fig. 2(b)], and the magnetoresistance peak at large angles is related to the sudden change of M_Z [see Supplemental Material [37] and Fig. 2S(b)] when the anisotropy energy barrier vanishes.

Most important, $MnBi_4Te_7$ undergoes a progressive transition at lower temperatures to a metamagnetic phase controlled by the uniaxial anisotropy. We evidence that this evolution of the total out-of-plane magnetization is related to that of the K/J ratio. Contrary to most uniaxial antiferromagnets, for which the exchange energy is much larger than the anisotropy, van der Waals–coupled magnetic multilayers can have competing energies, which results in specific magnetic properties. First, the spin-flop transition becomes hysteretic and two switching fields can be distinguished [Fig. 3(a)], as also observed by others [31]. As shown below by our model, this is due to the relative

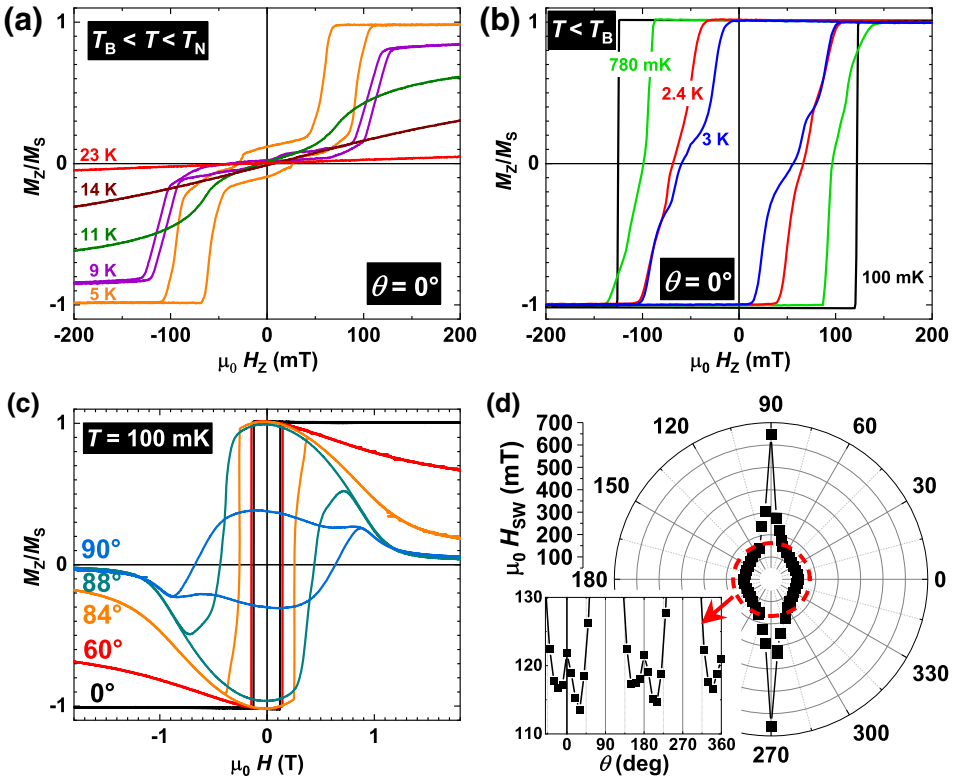

FIG. 3. Perpendicular magnetization M_Z hysteresis loops for $MnBi_4Te_7$, normalized to its saturation value M_S, showing (a) the split spin-flop transitions in the regime $K < 2J$ and (b) the evolution to a metamagnetic state ($K > 2J$) below the blocking temperature $T_B \approx 3$ K. Another narrower Hall bar shows a perfect spin-flip transition with a well-defined switching field, as shown at $T = 100$ mK. The angular dependence of hysteresis loops (c) reveals the dominant influence of the uniaxial anisotropy, with an anisotropy field $\mu_0 H_A \approx 0.7$ T. The Stoner-Wohlfarth mechanism is confirmed by (d) the polar plot of the switching field H_{SW} showing a truncated astroid behavior, with a maximum still clearly seen even along the easy axis (inset).

alignment of the sublattice magnetizations, which can be either parallel (P) or antiparallel (AP), resulting in two spin-flop fields H_{SF}^{AP} and H_{SF}^{P}. At 3K, the lower switching field H_{SF}^{P} changes its sign, and the remnant state becomes fully magnetized [Fig. 3(b)]. At very low temperatures, the hysteresis loop becomes very sharp with a single switching field [Fig. 3(c)], a behavior similar to that of a uniaxial ferromagnet. It is, however, the spin-flip transition of a metamagnetic state with a dominant uniaxial anisotropy energy ($K \gg J$), as confirmed by the angular dependence of M_Z [Fig. 3(c)]. Under a tilted field, the saturated magnetization rotates toward the magnetic field direction, and it is aligned for applied fields larger than the anisotropy field $\mu_0 H_A \approx 0.7$ T. The remnant magnetization remains fully saturated for nearly all angles, but for a large enough in-plane field that indeed cancels the energy barrier (which thus favors the decomposition in antiferromagnetic domains). Upon field reversal, the switching field H_{SW} is well defined and, after an initial decrease, it has a progressive angular dependence to a maximum value. This upper limit is due to the reduction of the anisotropy energy barrier under a transverse magnetic field. Indeed, the polar plot of H_{SW} shows the typical profile of a Stoner-Wohlfarth astroid [Fig. 3(d)], although it is truncated for small angles, when domain walls can be nucleated by a large enough H_Z component and the demagnetizing field.

All these experimental results can indeed be explained by a simple model based on two 2D ferromagnetic layers with a uniaxial perpendicular anisotropy K and adding a weak antiferromagnetic exchange coupling J, with competing interactions ($K \sim J$). This bilayer Stoner-Wohlfarth model allows us to describe the evolution from an A-type antiferromagnet to a uniaxial metamagnet, and it captures the temperature and angular dependences of the magnetization curves as well, given that K decreases with temperature. It also gives values of the K/J ratio required to stabilize each regime. We consider the free energy of two magnetic sublattices, each with a uniform magnetization $\vec{M}_{1,2} = M\vec{m}_{1,2}$, where $M = M_S/2$ and $\vec{m}_{1,2}$ are unit vectors. For a tilted magnetic field $\vec{H}$, with a polar angle θ with respect to the easy-anisotropy axis, each magnetic sublattice has an equilibrium state that can be obtained by minimizing the free energy, where two values θ_1 and θ_2 determine the sublattice magnetization orientations. The free energy reads $E = -\mu H[\cos(\theta_1 - \theta) + \cos(\theta_2 - \theta)] + K(\sin^2\theta_1 + \sin^2\theta_2) + 2J\cos(\theta_1 - \theta_2)$, where $\mu = \mu_0 M$.

Using the free energy, we can determine the magnetic ground state for each sublayer, as well as the energy barrier separating the parallel and antiparallel configurations (see Supplemental Material [37]). Neglecting thermal fluctuations (which contribute to a finite but small in-plane magnetic susceptibility), the total magnetization is thus calculated for any orientation and amplitude of the applied field.

To evidence the relative influence of the uniaxial anisotropy and of the antiferromagnetic interlayer exchange coupling, we consider the three limiting cases of a dominant exchange coupling ($K < 2J$), competing couplings ($K \approx 2J$), and a dominant uniaxial anisotropy ($K > 2J$). The magnetization curves along the anisotropy axis $M_z(H_z)$ are thus shown for three K/J ratios, representative of the different regimes.

We first focus on the regime $K/2J < 1$, for which spin-flop fields have the same sign. The ground state is that of a uniaxial antiferromagnet, with a zero net magnetization. By applying a magnetic field along the easy axis, there is a transition at H_{SF}^{AP}. Depending on the $K/2J$ ratio, the new equilibrium changes either to canted sublayer magnetization states or to a ferromagneticlike alignment in a finite field. For $K/2J < 1/3$ [Fig. 4(a)], the antiferromagnetic

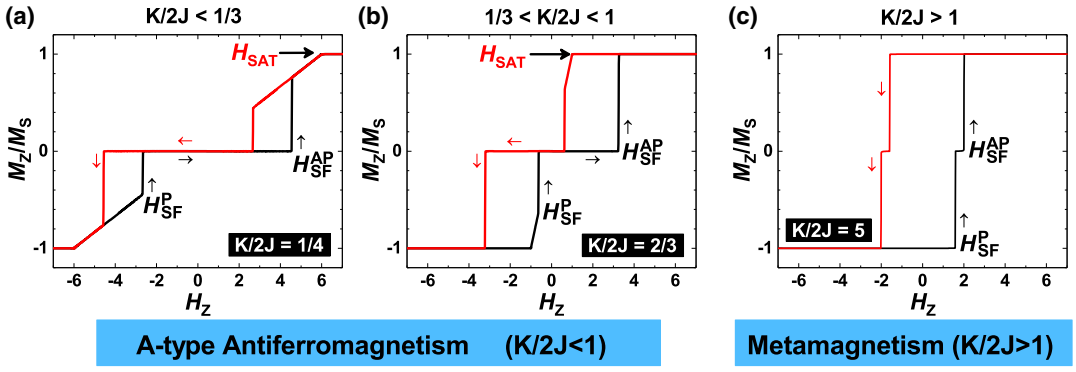

FIG. 4. Calculated hysteresis loops $M_Z(H_Z)$ for three $K/2J$ ratios ($\frac{1}{4}, \frac{2}{3}, 5$), representative of the different regimes. An A-type antiferromagnet with competing interactions has two spin-flop transition fields H_{SF}^{AP} and H_{SF}^{P}, depending on the relative alignment of the sublattice magnetizations. These can be smaller than the saturation field H_{SAT} [(a) dominant exchange energy] or give a larger hysteresis if the K/J ratio increases, with $H_{SAT} < H_{SF}^{AP}$ and reduced canting (b). The fully saturated metamagnetic state develops when the anisotropy energy becomes dominant (c), so that H_{SF}^{P} becomes negative and the magnetization switching proceeds as two spin-flip transitions (no canting) in a narrow field range. For a large enough K/J ratio, the magnetization reversal proceeds as a single spin-flip transition, only controlled by the uniaxial anisotropy.

ground state undergoes a spin-flop transition to a canted state. Increasing the field progressively brings the staggered magnetizations back to a parallel state, by coherent rotation (linear variation of the M_z component), with a full alignment at the saturation field $H_{SAT} \approx H_{exch}$. Because of the energy barrier, the spin-flop field depends on the relative orientation of the sublattice magnetizations (parallel P or antiparallel AP), which gives two different fields H_{SF}^{AP} and H_{SF}^{P}. For $1/3 < K/2J < 1$ [Fig. 4(b)], the antiferromagnetic ground state undergoes a spin-flip transition to a fully aligned state. This happens when H_{SAT} becomes smaller than H_{SF}^{AP} (decrease of J and/or increase of K).

Upon increasing the K/J ratio, the lower field H_{SF}^{P} is progressively reduced, as found in the intermediate regime of $MnBi_4Te_7$ (K increases at lower temperatures). For $K/2J = 1$, H_{SF}^{P} changes its sign, so that the remnant magnetization remains fully magnetized after an initial saturation. Because of the temperature dependence of K, this allows us to define a blocking temperature T_B as $H_{SF}^{P}(T_B) = 0$, the condition for a saturated remnant magnetization. By further increasing the K/J ratio [Fig. 4(c)], a larger hysteresis loop develops, as H_{SF}^{P} changed its sign and both spin-flop fields increase ($|H_{SF}^{P}|$ progressively increases faster, up to H_{SF}^{AP} in the $K \gg J$ limit). This is shown for $K/2J = 5$, where the magnetization reversal now proceeds as a narrow double step, which is then the spin-flip transition of a metamagnet. The limit $K/J \gg 1$ is the standard Stoner-Wohlfarth model with a single-step magnetization reversal, for which the switching field is solely controlled by the anisotropy barrier [as shown for $K/2J = 10$ in Supplemental Material [37], Fig. S6(b)].

This evolution is typical for the magnetic behavior found in $MnBi_4Te_7$ [Figs. 3(a) and 3(b)]. At very-low temperature, the magnetization reversal is a direct spin-flip transition that is mostly controlled by the anisotropy. This is confirmed by the angular dependence of the switching field that shows an astroidlike behavior [Fig. 3(d)], typical of magnetic systems with a uniaxial anisotropy. The asteroid is well reproduced in the hard-axis direction (evolution of the anisotropy energy barrier with an in-plane applied field), whereas it is truncated in the easy-axis direction, probably due to the formation of domain walls during the magnetization reversal in micron-sized magnets. Despite some intrinsic limitations of the single-domain approach [39], this bilayer model is very predictive since large domain sizes can be obtained in antiferromagnets, so that the free-energy description captures the physics of the competition between the uniaxial anisotropy and the interlayer antiferromagnetic exchange coupling.

In a comprehensive study of the magnetization reversal processes of magnetic topological insulators $MnBi_2Te_4$ ($n = 0$) and $MnBi_4Te_7$ ($n = 1$), we evidenced the anisotropy-controlled transition from an A-type collinear antiferromagnet to a fully saturated metamagnetic state in weakly coupled magnetic multilayers. Based on a simple Stoner-Wohlfarth model modified for a bilayer system with an antiferromagnetic exchange energy J, we reveal that ferromagneticlike hysteresis loops are actually the signature of a dominant anisotropy energy K, which offers the possibility to stabilize a uniform magnetization. Importantly, the detailed understanding of the different ground states of layered magnetic topological insulators is necessary so as to control novel topological states, induced by exchange fields, that can still be tunable by small external fields.

We acknowledge the funding of the European Commission via the TOCHA project H2020-FETPRO ACT-01-2018 under Grant Agreement No. 824140 and of the UGA IDEX IRS/PTISPIN. This work was supported by the German Research Foundation (DFG) in the framework of the SPP 1666 "Topological Insulators" program (IS 250/1-2 and DU 1376/2), of the CRC "Correlated Magnetism—From Frustration to Topology" (SFB-1143, Project No. 247310070), and of the Würzburg-Dresden Cluster of Excellence on Complexity and Topology in Quantum Matter—*ct.qmat* (EXC 2147, Project No. 39085490).

[1] R. Li, J. Wang, X.-L. Qi, and S.-C. Zhang, Nat. Phys. **6**, 284 (2010).
[2] R. S. K. Mong, A. M. Essin, and J. E. Moore, Phys. Rev. B **81**, 245209 (2010).
[3] K. Yasuda, M. Mogi, R. Yoshimi, A. Tsukazaki, K. S. Takahashi, M. Kawasaki, F. Kagawa, and Y. Tokura, Science **358**, 1311 (2017).
[4] L. Mejkal, Y. Mokrousov, B. Yan, and A. H. MacDonald, Nat. Phys. **14**, 242 (2018).
[5] C.-Z. Chang *et al.*, Science **340**, 167 (2013).
[6] A. J. Bestwick, E. J. Fox, X. Kou, L. Pan, K. L. Wang, and D. Goldhaber-Gordon, Phys. Rev. Lett. **114**, 187201 (2015).
[7] C.-Z. Chang, W. Zhao, D. Y. Kim, H. Zhang, B. A. Assaf, D. Heiman, S.-C. Zhang, C. Liu, M. H. W. Chan, and J. S. Moodera, Nat. Mater. **14**, 473 (2015).
[8] M. Götz, K. M. Fijalkowski, E. Pesel, M. Hartl, S. Schreyeck, M. Winnerlein, S. Grauer, H. Scherer, K. Brunner, C. Gould, F. J. Ahlers, and L. W. Molenkamp, Appl. Phys. Lett. **112**, 072102 (2018).
[9] E. J. Fox, I. T. Rosen, Y. Yang, G. R. Jones, R. E. Elmquist, X. Kou, L. Pan, K. L. Wang, and D. Goldhaber-Gordon, Phys. Rev. B **98**, 075145 (2018).
[10] M. M. Otrokov, T. V. Menshchikova, I. P. Rusinov, M. G. Vergniory, V. M. Kuznetsov, and E. V. Chulkov, JETP Lett. **105**, 297 (2017).
[11] M. M. Otrokov, T. V. Menshchikova, M. G. Vergniory, I. P. Rusinov, A. Y. Vyazovskaya, Y. M. Koroteev, G. Bihlmayer, A. Ernst, P. M. Echenique, A. Arnau, and E. V. Chulkov, 2D Mater. **4**, 025082 (2017).
[12] J. Li, Y. Li, S. Du, Z. Wang, B.-L. Gu, S.-C. Zhang, K. He, W. Duan, and Y. Xu, Sci. Adv. **5**, 6 (2019).
[13] Y. Tokura, K. Yasuda, and A. Tsukazaki, Nat. Rev. Phys. **1**, 126 (2019).
[14] M. M. Otrokov *et al.*, Nature (London) **576**, 416 (2019).

[15] Y. Gong, Chin. Phys. Lett. **36**, 076801 (2019).
[16] S. H. Lee, Y. Zhu, Y. Wang, L. Miao, T. Pillsbury, H. Yi, S. Kempinger, J. Hu, C. A. Heikes, P. Quarterman, W. Ratcliff, J. A. Borchers, H. Zhang, X. Ke, D. Graf, N. Alem, C.-Z. Chang, N. Samarth, and Z. Mao, Phys. Rev. Research **1**, 012011(R) (2019).
[17] J.-Q. Yan, Q. Zhang, T. Heitmann, Z. Huang, K. Y. Chen, J.-G. Cheng, W. Wu, D. Vaknin, B. C. Sales, and R. J. McQueeney, Phys. Rev. Mater. **3**, 064202 (2019).
[18] B. Chen *et al.*, Nat. Commun. **10**, 4469 (2019).
[19] P. Baireuther, J. M. Edge, I. C. Fulga, C. W. J. Beenakker, and J. Tworzydło, Phys. Rev. B **89**, 035410 (2014).
[20] M. M. Otrokov, I. P. Rusinov, M. Blanco-Rey, M. Hoffmann, A. Y. Vyazovskaya, S. V. Eremeev, A. Ernst, P. M. Echenique, A. Arnau, and E. V. Chulkov, Phys. Rev. Lett. **122**, 107202 (2019).
[21] H. Sun, B. Xia, Z. Chen, Y. Zhang, P. Liu, Q. Yao, H. Tang, Y. Zhao, H. Xu, and Q. Liu, Phys. Rev. Lett. **123**, 096401 (2019).
[22] D. Zhang, M. Shi, T. Zhu, D. Xing, H. Zhang, and J. Wang, Phys. Rev. Lett. **122**, 206401 (2019).
[23] J. Li, C. Wang, Z. Zhang, B.-L. Gu, W. Duan, and Y. Xu, Phys. Rev. B **100**, 121103(R) (2019).
[24] Y. Deng, Y. Yu, M. Z. Shi, Z. Guo, Z. Xu, J. Wang, X. H. Chen, and Y. Zhang, Science **367**, 895 (2020).
[25] C. Liu, Y. Wang, H. Li, Y. Wu, Y. Li, J. Li, K. He, Y. Xu, J. Zhang, and Y. Wang, Nat. Mater., https://doi.org/10.1038/s41563-019-0573-3, 2020.
[26] J. Ge, Y. Liu, J. Li, H. Li, T. Luo, Y. Wu, Y. Xu, and J. Wang, National Science Review, https://doi.org/10.1093/nsr/nwaa089, 2020.
[27] C. Hu, K. N. Gordon, P. Liu, J. Liu, X. Zhou, P. Hao, D. Narayan, E. Emmanouilidou, H. Sun, Y. Liu, H. Brawer, A. P. Ramirez, L. Ding, H. Cao, Q. Liu, D. Dessau, and N. Ni, Nat. Commun. **11**, 97 (2020).
[28] R. C. Vidal *et al.*, Phys. Rev. X **9**, 041065 (2019).
[29] J. Q. Yan, Y. H. Liu, D. Parker, M. A. McGuire, and B. C. Sales, arXiv:1910.06273.
[30] M. Z. Shi, B. Lei, C. S. Zhu, D. H. Ma, J. H. Cui, Z. L. Sun, J. J. Ying, and X. H. Chen, Phys. Rev. B **100**, 155144 (2019).
[31] J. Wu, F. Liu, M. Sasase, K. Ienaga, Y. Obata, R. Yukawa, K. Horiba, H. Kumigashira, S. Okuma, T. Inoshita, and H. Hosono, Sci. Adv. **5**, eaax9989 (2019).
[32] L. X. Xu *et al.*, arXiv:1910.11014.
[33] I. I. Klimovskikh *et al.*, arXiv:1910.11653.
[34] M. Gibertini, M. Koperski, A. F. Morpurgo, and K. S. Novoselov, Nat. Nanotechnol. **14**, 408 (2019).
[35] A. Zeugner *et al.*, Chem. Mater. **31**, 2795 (2019).
[36] D. Souchay, M. Nentwig, D. Günther, S. Keilholz, J. de Boor, A. Zeugner, A. Isaeva, M. Ruck, A. U. B. Wolter, B. Büchner, and O. Oeckler, J. Mater. Chem. C **7**, 9939 (2019).
[37] See Supplemental Material at http://link.aps.org/supplemental/10.1103/PhysRevLett.124.197201 for more details on experiments, the magnetic configurations and the bilayer Stoner-Wohlfarth model.
[38] J. M. D. Coey, *Magnetism and Magnetic Materials* (Cambridge University Press, Cambridge, England, 2010).
[39] B. Dieny, J. P. Gavigan, and J. P. Rebouillat, J. Phys. Condens. Matter **2**, 159 (1990).